Int. J. Rock Mech. Min. Sci. & Geomech. Abstr. Vol. 20, No. 6, pp. 249–268, 1983
Printed in Great Britain. All rights reserved

0148-9062/83 $3.00 + 0.00
Copyright © 1983 Pergamon Press Ltd

Fundamentals of Rock Joint Deformation

S. C. BANDIS*
A. C. LUMSDEN†
N. R. BARTON‡

This paper describes laboratory investigations of the deformation characteristics of rock joints under normal and shear loading. Normal deformability was studied by conducting loading/unloading and repeated load cycling tests on a wide variety of fresh and weathered joints in five different rock types. The data invariably showed non-linear behaviour, irrespective of the rock and joint type. A hyperbolic function is suggested to describe the stress–closure/opening curves of joints. Quantitative relations between normal deformability and revelant joint parameters (aperture, wall strength and roughness) are developed. Tentative conclusions on the changes in normal stiffness during shearing are also presented. The behaviour of dislocated (mismatching) joints is studied qualitatively and analytically. Shear deformability was studied by performing direct shear tests under normal stresses in the range of engineering interest. It is shown that behaviour in the pre-peak range is invariably non-linear depending on the joint type, and can be adequately described by easily measured parameters and hyperbolic functions.

INTRODUCTION

Joint deformation is a fundamental component of the performance of a discontinuous rock mass under changing stress conditions. At the relatively low stress levels encountered in near-surface excavations, the deformation of joints dominates the elastic deflection of the intact rock. Even under the higher levels of stress associated with heavy structures, the slippage and closure of joints constitute the major part of settlement on rock.

Joint deformability can be described by the character of the stress–deformation curves. Goodman *et al.* [1] introduced the terms "normal stiffness" (K_n) and "shear stiffness" (K_s) to describe the rate of change of normal stress (σ_n) with respect to normal displacements (V_j) and of the shear stress (τ) with respect to shear displacements (d_h) respectively. The above quantities, together with values for peak (d_{hp}) and residual (d_{hr}) shear displacement and maximum joint closure (V_m), allow computation of the contribution of joints to the total displacement of the rock mass.

Goodman [2] described the basic mechanics of joint normal deformation by considering that the maximum closure (V_m) of a joint should be less than its aperture thickness (a_j), defined as the maximum gap anywhere across the mated walls. Goodman's experiments showed that the joint closure (ΔV_j) under increasing normal stress (σ_n) varies in a non-linear fashion closely resembling a hyperbola. A characteristic example is illustrated in Fig. 1. The non-linearity in the σ_n–ΔV_j relations was also recognized by other workers [3–5]. On the other hand, some tests by Hungr and Coates [6] gave virtually linear σ_n–ΔV_j relations at low σ_n levels. The authors attributed that behaviour to a "precompression" effect. Snow [7] noted that non-linear behaviour is related to "normally compressed" joints (i.e. a condition equivalent to normal consolidation of clays).

The factors which may be expected to influence the normal stiffness of joints are:

(i) initial actual contact area, relative amplitude and vertical distribution of the aperture between the joint walls;

(ii) joint wall roughness (in the authors' view the small scale roughness is the most critical in controlling normal stiffness. It is unlikely that joint closure is size-dependent);

(iii) strength and deformability of asperities;

(iv) thickness, type and physical properties of the infilling material, if present (e.g. Infanti and Kanji [8]).

Factual information regarding the effects of joint wall strength, roughness, aperture, etc. on the normal stiffness of unfilled joints is rather limited. This is largely because most of the relevant studies have been conducted on artificial fractures, which resembled only certain types of natural joints, and have presented a restricted range of the variables in question.

More information can be found concerning the property shear stiffness (e.g. see the review by Kulhaway [10]). Comparison between the pre-peak portions of shear stress (τ)–shear displacement (d_h) curves indicates both linear and non-linear behaviour. The latter is often

* 83 Kassandrou Street, Thessaloniki, Greece.
† Department of Earth Sciences, University of Leeds, Leeds LS2 9JT, U.K.
‡ Terra Tek Inc., University Research Park, 400 Wakara Way, Salt Lake City, UT 84108, U.S.A.

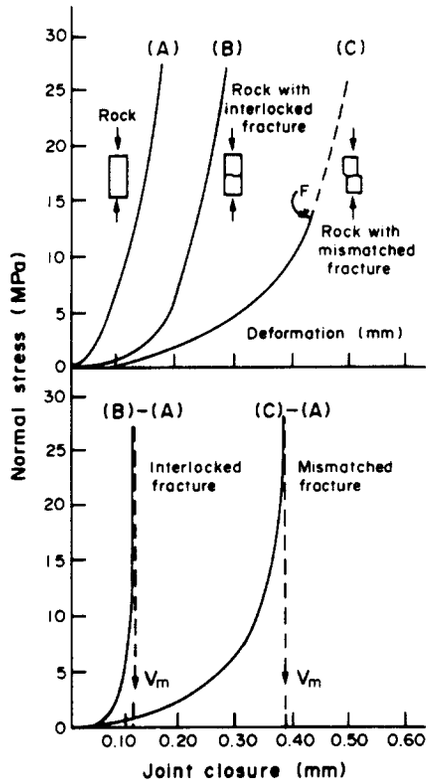

Fig. 1. Normal stress vs deformation relations of intact and fractured cylindrical specimens of granodiorite [9].

modelled by the use of simple hyperbolic functions. The shear stiffness parameter K_s generally increases with increasing σ_n, although a "constant peak displacement" model [11] is not always realistic. It may also be difficult to make strictly valid comparisons between various test cases, as the K_s values are affected by the experimental technique [12]. Finally, K_s depends on the size of the sample tested [13].

Both the normal and shear stiffness parameters (K_n and K_s) are fundamental input data for explicit physical models and numerical approximation techniques. Also, joint normal stiffness is fundamentally linked with the problems of fluid injection into or withdrawal from jointed rock. Thorough understanding of the deformational response of rock joints in relation to varying roughness, wall strength and aperture is essential in the study of rock mass permeability.

This paper presents the findings of a laboratory investigation on the deformational behaviour of a wide ranging variety of nature unfilled joints. The objectives of these experiments may be summarized as:

(i) Investigation of the complete stress–deformation relation of different joint types under loading/unloading and repeated load cycle conditions.

(ii) Definition of an analytical representation of the deformation curves.

(iii) Study of the effects of joint weathering on normal stiffness.

(iv) Derivation of empirical relations of possible practical value between deformability parameters and basic joint variables.

(v) Comparative study of the deformational characteristics of joints "displaced" in shear.

EXPERIMENTAL WORK

Fresh and weathered joint samples were collected from exposures in the UK of five rock types, namely slate, dolerite, limestone, siltstone and sandstone. Some index properties of the fresh rock materials are given in Table 1.

The normal deformability tests involved cyclic loading of single-jointed rectangular blocks with side lengths 80–100 mm, widths 40–60 mm and heights 50–70 mm and were conducted on a 50-ton Dennison compression machine. Both the loading ends of each test block were subjected to several stages of progressively finer grinding and were finally polished on a lapping wheel using a 600 grade silicon carbide. For all samples it was ensured that the average joint plane was aligned in a position parallel to the loading ends of the blocks to within 1°–2°.

The prepared joint blocks were compressed between two accurately machined hardened steel platens. The vertical displacements under normal loading or unloading were recorded by two sensitive dial gauges to an accuracy of $\pm 0.5 \times 10^{-3}$ mm. The dial gauges were connected to magnetic stands seated on the basal platen.

Table 1. Index properties and sampling locations

Rock materials \ Properties	Tensile strength σ_t (MPa)	Compressive strength σ_c (MPa)	Young's modulus $E_{150\sigma_c}$ (GPa)	Unit weight γ(KN/m^3)
Slate (Ordovician from Skiddaw Slates—Quarry nr Keswick, Lake District)	14.9	159.0	66.0	27.7
Dolerite (Permo-Carboniferous —natural exposure at Horwick Crags, Teesdale)	17.3	165.0	78.0	29.0
Limestone (Lower Carboniferous —natural exposure, N. Yorks)	10.6	152.0	49.0	27.3
Siltstone (Upper Coal Measures —NCB pit, W. Yorks)	6.3	84.0	28.5	24.2
Sandstone (Lower Coal Measures —Shibden Dale Quarry, W. Yorks)	5.1	78.0	24.0	24.1

The spindles of the gauges were brought to rest vertically on two laterally projecting horizontal aluminium platelets, which were fixed directly on the two opposite ends of the upper block-half and in the middle. An average value of displacement was calculated from the readings of the two gauges at each increment or decrement of normal load.

Direct shear tests were conducted in a portable shear apparatus. The normal and shear loads were applied by means of wire ropes and hydraulic rams. The pump feeding the normal loading ram was fitted with an adjustable low friction pressure maintainer, thus allowing constant normal loading conditions during testing of dilatant surfaces. The shear tests were conducted by following an incremental multistage procedure. At the end of each run the joint sample was reassembled to its original position before starting a new shear run under higher normal load.

In order to ensure accurate measurements of shear displacements, the hydraulic ram for shear reversal was removed from the lower box-half and two dial gauges were fitted at an appropriate height so that their spindles could go through the existing holes of the ram screws. By attaching an extension to the standard spindle length, the ends were brought to rest on the two corners of the upper joint block-half at a distance of 1–2 mm above the shear plane. Average values were used in the plotting of the shear stress–shear displacement diagrams.

Description and index properties of joints

The joint samples were extracted from the rock exposures manually with the aid of a hammer and chisel. Maximum care was taken to avoid accidental damage of the joint walls, by "releasing" the block to be sampled as much as possible from the surrounding rock prior to extraction, and then wiring the two halves safely together for transportation.

Descriptions of the various joints types are presented in Table 2. Explanation of the symbols and other details are given below:

(i) *Joint Types*: IF = joint induced along a natural incipient fracture; CP = cleavage plane; VJ = vertical joint; BP = bedding plane; AF = artificial extension fracture

(ii) *Weathering State*: The various samples are described as fresh (F), slightly weathered (SW), moderately weathered (MW) and weathered (W), according to their relative weathering, quantified by the σ_c/JCS ratio values (where JCS is the joint compressive strength estimated by direct Schmidt hammer testing of the surfaces and σ_c is the uniaxial compressive strength estimated by Schmidt hammer tests on perfectly fresh samples of each rock type). The ranges of description are as follows:

F to SW: $\sigma_c/\mathrm{JCS} \leqslant 1.2$
MW: $1.2 < \sigma_c/\mathrm{JCS} \leqslant 2$
W: $\sigma_c/\mathrm{JCS} > 2$

(iii) *Joint Wall Strength*: R = mean rebound number from Schmidt hammer (L-type) tests on dry joint surfaces; γ = mean unit weight of joint wall material; JCS = mean joint compressive strength calculated from $\log_{10} \mathrm{JCS} = 0.00088 \cdot \gamma \cdot \mathrm{R} + 1.01$.

(iv) *Joint Wall Geometry*: The profiles give representative examples of the range of roughness for each group of joints; JRC = joint roughness coefficient obtained from direct shear tests under $\mathrm{JCS}/\sigma_n \cong 2000$; JRA = joint roughness amplitude measured on the joint profile as the average vertical amplitude of the prominent surface protrusions; a_j = average aperture values for each group of joints measured with feeler gauges.

Normal deformation of interlocked joints

A total of 64 interlocked jointed block samples were subjected to a sequence of loading/unloading cycles. The total deformation (ΔV_t) was recorded at regular increments or decrements of normal stress (σ_n). All compression tests were conducted from an initial stress level (σ_i) of approximately 1 kPa. The maximum applied stresses ranged from approximately 5–10 MPa to 50–55 MPa, which corresponded to 1/3–1/2 of the uniaxial compressive strength (σ_c) of the various rock materials. Such high stress levels ensured almost complete closure of the joints.

The normal stress (σ_n) vs total deformation (ΔV_t) curves of the various joint block samples invariably showed non-linear behaviour within a wide range of stresses. Two typical examples are shown in Fig. 2. At the initial loading states, the deformation (ΔV_t) of the joint blocks was dominated by the displacements occurring across the joint interface. For instance, it was estimated that during the first loading and under $\sigma_n = 1.0$ MPa, the average value of the ratio of total deformation (ΔV_t) to rock compression (ΔV_r) ranged between 5 and 30 depending on the rock type and the weathering state of the joint. Under increasing σ_n the curves became gradually steeper and in most cases developed into virtually straight lines, which were parallel, or nearly parallel to the elastic compression curves of the solid rock. It is generally considered that at this stage the joints have closely approached or reached their fully closed state and that any further increase in normal load is taken up by the solid rock above and below the joint. On decompression, all joint blocks showed markedly hysteretic behaviour, and upon return to the initial stress level (σ_i), a large amount of permanent set was observed. Reloading for the second and third time produced much steeper curves, while each unloading persistently showed hysteresis and inelasticity.

The normal stress (σ_n) vs net deformation or closure (ΔV_j) curves were derived from:

$$\Delta V_j = \Delta V_t - \Delta V_r \tag{1}$$

where ΔV_t was the total deformation of the joint block under σ_n during loading or unloading and ΔV_r was the corresponding deformation of the solid rock (separately measured on "identical" intact samples). Some typical curves are given in Figs 3 and 4 for a range of fresh and weathered joint types.

The σ_n–ΔV_j curves, especially those of the fresh joints,

Table 2. Summary of the physical characteristics of the various joint types

Joint types and (no.) of samples	General description	Weathering state	Joint wall strength: R	Joint wall strength: γ (kN/m^3)	Joint wall strength: JCS (MPa)	Joint wall geometry: Typical range of roughness profiles (0 1 2 3 4 5 6 7 8 9 10 scale (cm))	a_j (mm)	JRC	JRA (mm)
					Slate				
IF (3)	Well interlocked planar cleavage fractures	[F]	50.6	27.7	175		~0.10	4–5	0.80 0.93
CP (1)	Walls completely discolored to yellow-brown	[MW]	42.5	27.82	122		0.15	5.3	1.20
CP (3)	Walls covered by thin film of limonite and weathered calcite. Poor locking	[W]	36.8	27.05	77		0.50	6.0– 6.8	0.95– 1.50
					Dolerite				
VJ (2)	Slight discoloration to yellow-brown in places	[F]–[SW]	47.5– 49.0	29.0	167– 182		0.15– 0.20	6.1– 8.8	0.90– 1.65
VJ (3)	Surfaces covered by limonite 2–3 mm of wall rock discolored to yellowish poor locking	[W]	32.4– 36.9	26.75– 26.92	60– 76		0.50– 0.60	6.0– 8.7	1.0– 2.7
					Limestone				
BP & VJ (11)	Surfaces partially (5–50%) to completely discolored to yellowish. All samples well interlocked	[F]–[SW]	49.1– 50.2	26.95– 27.27	152– 170		0.20– 0.25	5.6– 11.4–	1.0– 3.4

BP & VJ (5)	Surfaces discolored to darker gray and porous, or heavily stained with softer porous patches. Well locked	[MW]	40.6–45.0	26.80–26.97	94–120	0.20	5.8–15.0	1.6–7.8
VJ (5)	Joints covered by crust (~0.5 mm) of yellowish, porous, weak weathered material. Poor locking	[W]	23.6–30.5	25.20–25.68	35–50	0.40–0.50	5.0–16	1.1–8.2
					Silstone			
AF (5)	Rough extension fractures vertical to bedding	[F]	47.5	24.20	105	0.15	8.0–1.8	2.5–4.5
BP (5)	Surfaces partially (40–60%) or completely discolored to yellow-brown (rusty) and flaky. Poorly locked	[MW]–[W]	29.3–39.3	23.62–23.80	42–67	0.60	6.1–7.5	1.6–2.2
					Sandstone			
BP & VJ (8)	Surfaces perfectly fresh or covered by a thin, dark brown, hard crust of iron oxides. Well locked	[F]–[SW]	38.8–44.4	24.1–24.75	74–95	0.20–0.25	5.4–11.9	0.8–3.8
JBP & VJ (9)	Surfaces partially (20–40%) or completely stained. Rock material slightly discolored (grade II). Well locked	[MW]	30.1–36.0	23.80–23.92	44–58	0.25	5.1–14.1	0.9–5.4
BP (4)	Rock material highly weathered throughout (grade IV). Complete discoloration into brown. Bedding planes poorly locked	[W]	19.0–22.2	19.90	22–25	0.40–0.60	5.0–6.0	0.9–1.8

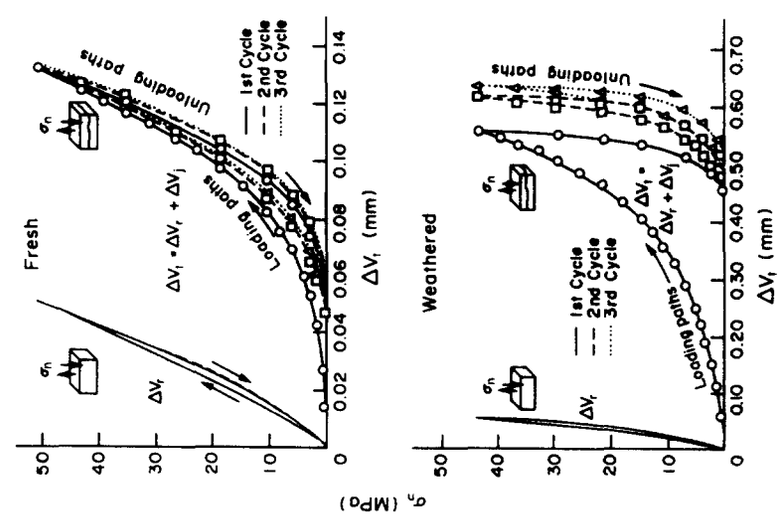

Fig. 2. Normal stress (σ_n) vs total deformation (ΔV_t) relations for fresh and weathered joints in dolerite under repeated loading cycles. The solid rock compression curves (ΔV_i) were derived from separately tested intact samples of the same dimensions.

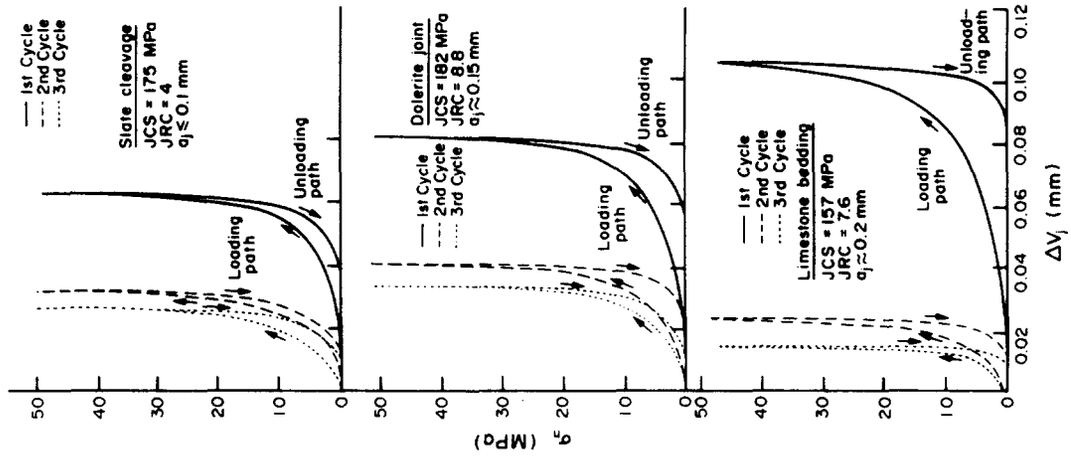

Fig. 3. Normal stress (σ_n) vs closure (ΔV_j) curves for a range of *fresh* joints in different rock types, under repeated loading cycles.

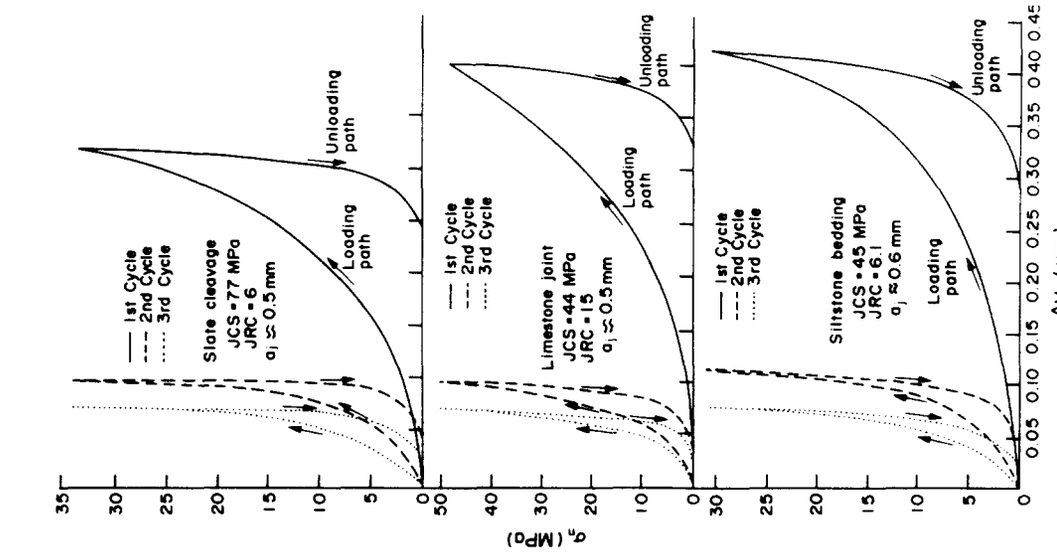

Fig. 4. normal stress (σ_n) vs closure (ΔV_j) curves for a range of *weathered* joints in different rock types under repeated loading cycles.

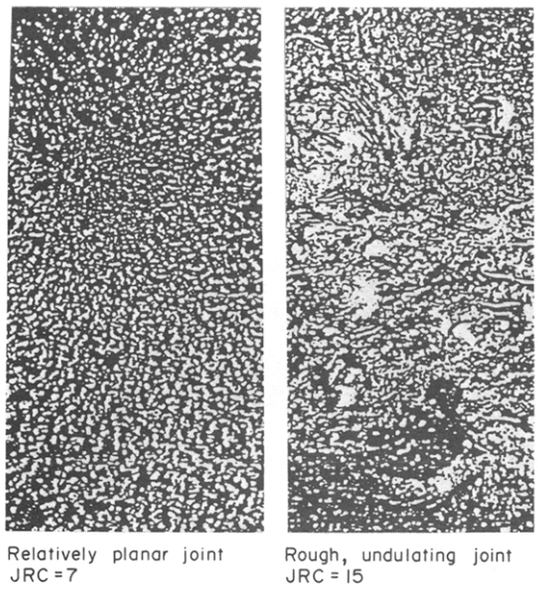

Fig. 5. Illustration of the variation and distribution of actual contact areas (white coloured features) of two interlocked limestone joints under normal stresses of 35 MPa. (Note: the insert was a "Melinex" polyester film 12 μm in thickness manufactured by ICI).

resembled a hyperbola. Under very high stresses, the paths became asymptotic to a vertical line, which represented the limit of joint closure (V_{max}). The closure curves of the weathered joints were often more "open" during the first loading. The apparent state of maximum closure for the latter was usually reached after the 2nd or 3rd loading.

Despite the very high stresses applied, the actual contact area between the walls ranged between approximately 40 and 70% of the total sample area, depending on JCS and JRC. A characteristic illustration is shown in Fig. 5. The impressions of the contacts were obtained by inserting an extremely thin plastic sheet between the interlocked joint walls. It is interesting to note the uniform size and distribution of the contacts on the relatively planar joint, as compared to the relatively random pattern and variability of the contacts on the rough, undulating joint. The continuity in the complex system of "channels" explains the observed flow of water through single fractures under extremely high σ_n [5].

In general, the current observations on the deformation characteristics of a wide variety of natural joint types, agree qualitatively with earlier findings from tests on artificial fractures. As noted earlier, the stress–closure relations for a number of natural limestone and sandstone joints were interpreted as close to linear [6] due to previous *in-situ* compression under stresses much higher than those applied in the tests (up to $\cong$2.5 MPa). Although it is undoubtedly correct that joint deformability depends on the previous stress history, the level of σ_n in those tests was too low to reveal the complete joint behaviour.

Furthermore, the inevitable disturbance of the natural *in-situ* closure and seating condition was seemingly not taken into account. "Precompression" effects can only be studied conclusively, if such conditions are adequately reproduced prior to the test. It should be noted that even extremely tightly locked joints showed non-linear behaviour after two cycles under very high stresses.

Normal deformation of dislocated joints

Compression tests were conducted on a range of dislocated joints. The two block halves of each sample were relatively displaced by $\cong$0.5–1.0 mm, thus approximating the usual shear displacement of joints at peak strength in the present length range. For some joints, a slight rotation about a vertical axis was necessary to avoid imbalance and rotation during loading. The average opening (d_v) across the mismatched interfaces ranged from 0.15 to 1.30 mm depending on the surface roughness. The maximum applied stresses usually approached 1/3 of the uniaxial compression strength of the rock. The initial stress level was approximately 0.15 MPa.

The normal stress (σ_n) vs closure (ΔV_j) curves of the dislocated joints revealed similar behaviour as when loaded in a fully locked position, following non-linear loading paths, and showed typical hysteretic recovery

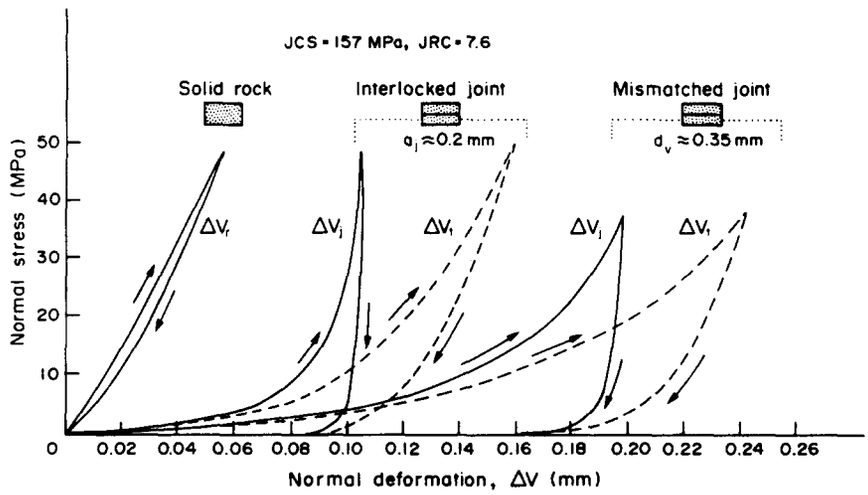

Fig. 6. Comparison of total deformation (ΔV_t) and net closure curves $\Delta V_j = \Delta V_t - \Delta V_r$) from the first loading cycle of the same joint tested in fully interlocked and mismatched positions.

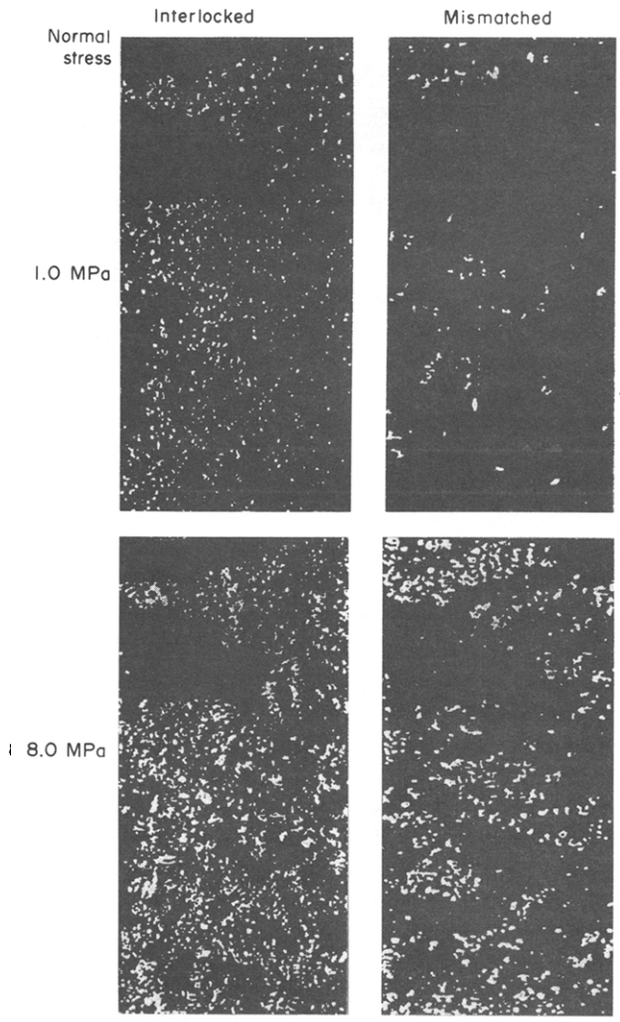

Fig. 7. Comparison of the size and distribution of the actual contact area (white coloured features) of a sandstone joint, compressed in interlocked and mismatched positions under two levels of normal stress. (Note: the impressions of the contact areas were taken in the same manner as described in Fig. 5).

and huge permanent set. The factors which controlled the amount of closure were the joint opening (d_v), the surface roughness (JRC) and the mechanical strength (JCS) of the asperities in contact. A typical test case is presented in Fig. 6, where the total deformation (ΔV_t) and closure (ΔV_j) curves of a limestone joint compressed in interlocked ($a_j = 0.20$ mm) and mismatched ($d_v = 0.35$ mm) positions are compared. The much lower stiffness of the mismatched joint is the expected result of stress concentration over a lower actual contact area and the lack of asperity confinement. (An example is shown in Fig. 7).

Shear deformation

The shear deformability up to mobilization of peak strength was studied for a range of fresh and weathered joint types. Typical shear stress (τ) vs displacement (d_h) curves are given in Fig. 8. All types of joint exhibited non-linear behaviour to a greater or lesser extent. An exception was the case of extremely tight natural induced cleavage fractures in slate, which showed virtually linear behaviour. The peak shear displacement (d_{hp}) of weathered joints was considerably larger than that of fresh joints due to poor interlocking and relatively planar geometry. Depending on σ_n, the peak shear stiffness (K_s) of weathered joints was 2–4 times lower than the K_s of fresh samples with similar JRC. As expected, K_s was found to depend on σ_n irrespective of the type of joint.

The practical relevance of the shear stiffness (K_s) values determined from small samples depends on the lengths of joints involved in a particular problem. Significant scale effects have been found in both the peak shear strength (τ_p) and displacement (d_{hp}) of model joints (Bandis *et al.* [15]). A plot summarizing the scale effect on K_s is presented in Fig. 9, which comprises some 450 data from the literature representing a wide range of discontinuities.

Another factor potentially affecting the peak shear stiffness of a joint is its past loading history. The effects of "overclosure" on the peak shear resistance have been demonstrated in the past [16]. Shear loading of two weathered sandstone joints under σ_n of 2 MPa showed

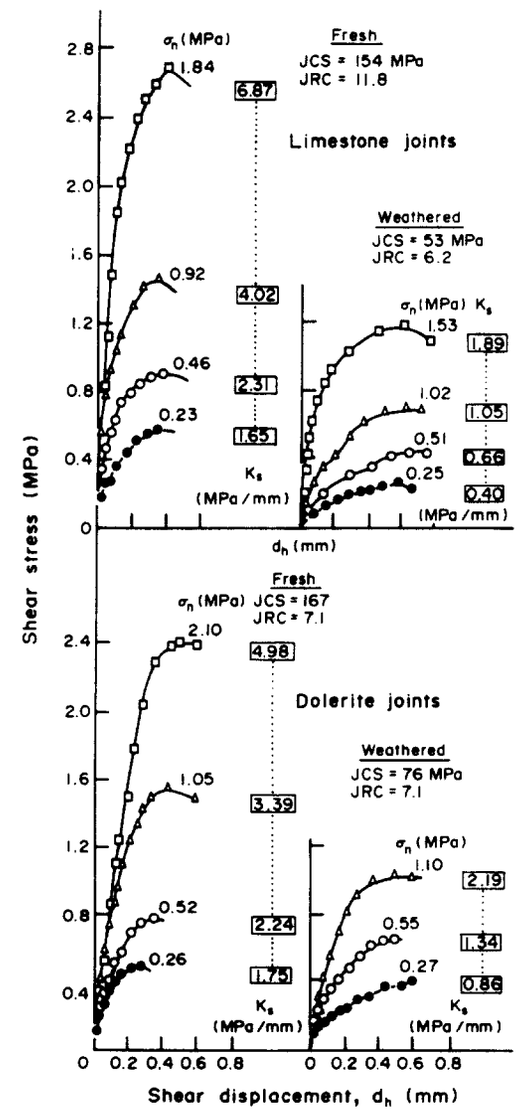

Fig. 8. Shear stress (τ) vs displacement (d_h) curves for fresh and weathered joints at various normal stress (σ_n) levels. Secant peak shear stiffness (K_s) values are also included.

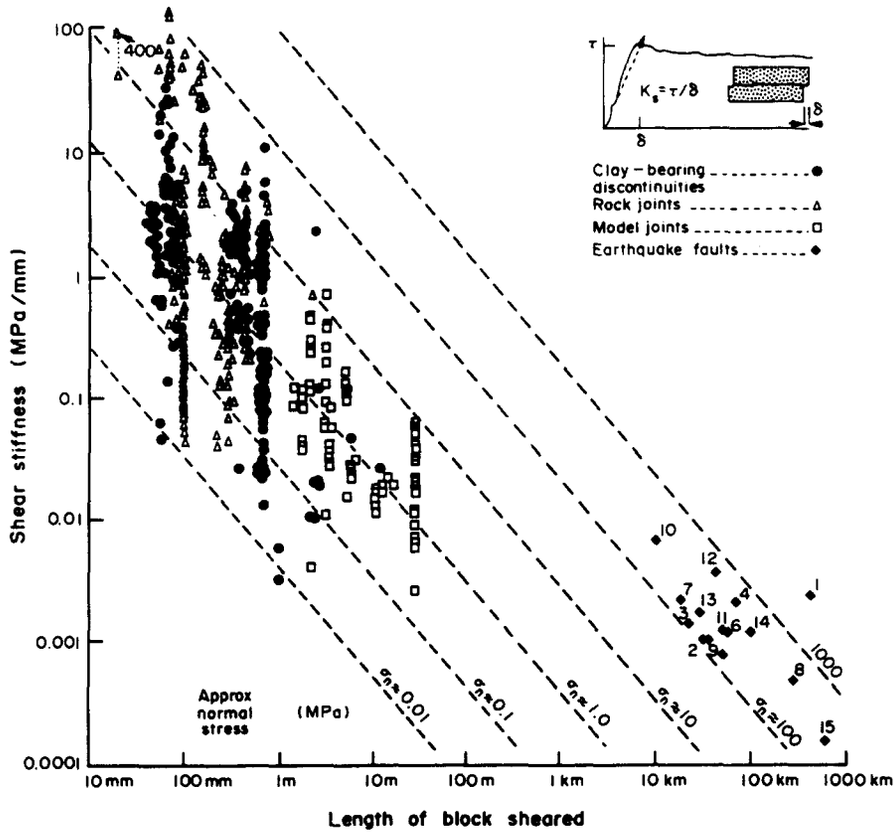

Fig. 9. Experimental evidence for the scale effect on peak shear stiffness. The normal stress diagonals were tentatively extrapolated from tests at 100 mm size, from the measured effects of scale on JRC, JCS and d_h in the 100 mm to 1 m size range.

an approximately 3-fold increase in K_s when subjected to an overclosure ratio of 7:1 (Fig. 10).

ANALYSIS OF THE STRESS–DEFORMATION RELATIONS

(*a*) *Normal stress* (σ_n) *vs closure* (ΔV_j) *curves*

(*i*) *Interlocked joints*. The normal loading tests have demonstrated that the σ_n–ΔV_j relations for a wide range of natural, unfilled joint types are invariably non-linear throughout repeated loadings.

Shehata [3] has described the above relation as being semi-logarithmic. Plots of ΔV_j data vs logarithmically scaled σ_n, showed a linear fit in the low and high stress regions, but not in the medium stress range. The plots for the loading paths from subsequent cycles were generally linear over a wider range of σ_n. Non-linearity over the medium stress range was also observed in the semi-log plots of the unloading paths.

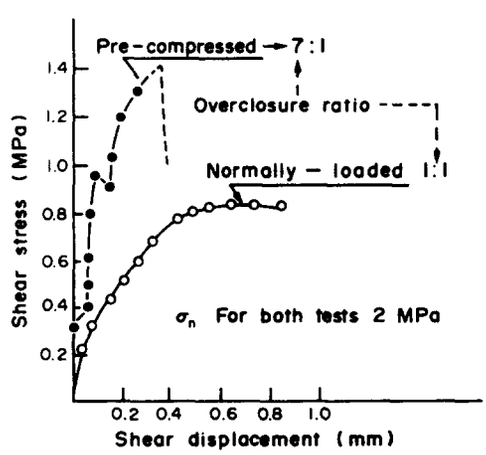

Fig. 10. Illustration of the effects of overclosure upon the shear strength and deformability of two weathered sandstone joints.

Goodman [2] proposed the empirical hyperbolic function:

$$\sigma_n = \left(\frac{\Delta V_j}{V_m - \Delta V_j}\right)\sigma_i + \sigma_i \tag{2}$$

which can be rearranged in the following linear form:

$$\Delta V_j = V_m - (V_m \sigma_i)\frac{1}{\sigma_n} \tag{3}$$

where, ΔV_j is the joint closure under a given σ_n, V_m is the maximum closure and σ_i is the initial stress level. Plots of ΔV_j vs $1/\sigma_n$ showed marked non-linearity except in the low stress region. An alternative version of function (2) was given by Goodman [9] in the following dimensionless form:

$$\frac{\sigma_n - \sigma_i}{\sigma_i} = C\left[\frac{\Delta V_j}{V_m - \Delta V_j}\right]^t \tag{4}$$

where C and t are constants. Trials of function (4) showed a conversion of the highly non-linear relation of ΔV_j vs $1/\sigma_n$ to near perfect bilinear curves due to the logarithmic formulation. Typical examples of the fitting

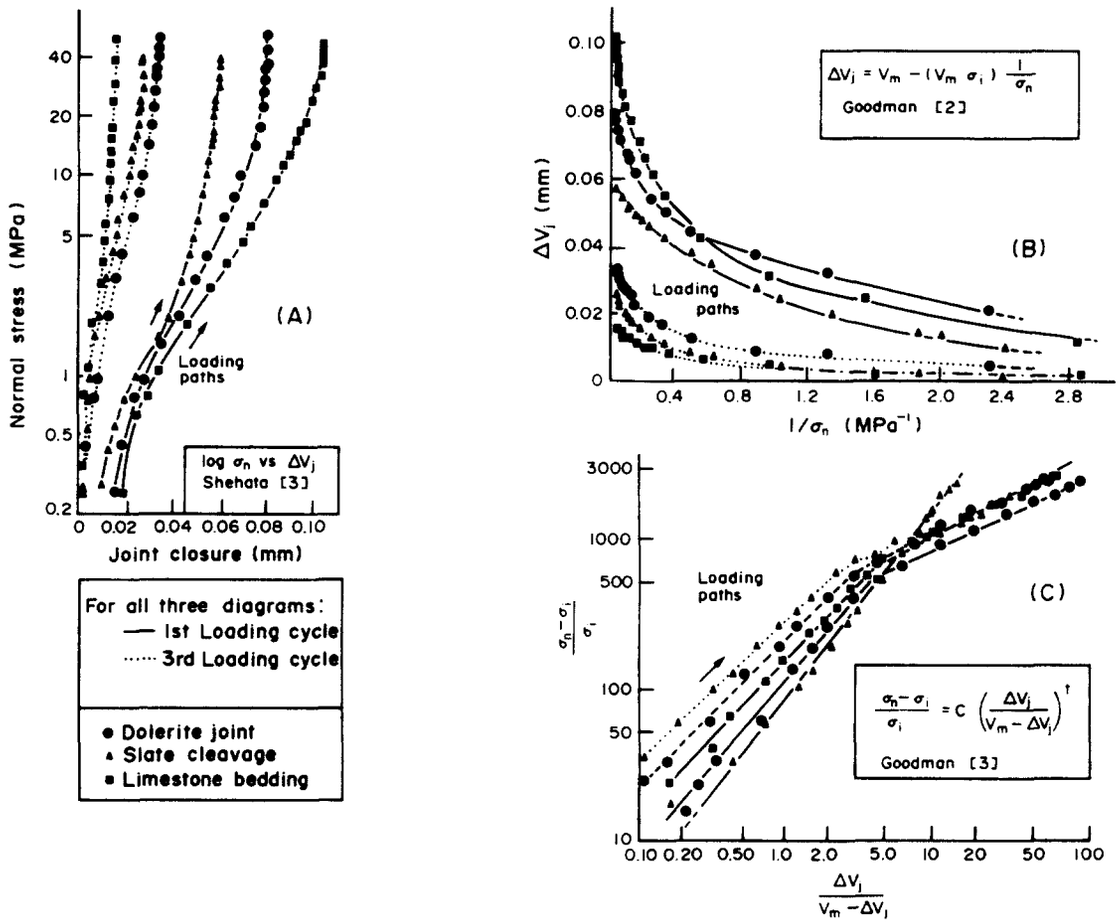

Fig. 11. Comparison of the fitting potential of various empirical functions to the loading curves of rock joints.

discrepancies of the above described functions are compared in Fig. 11 for three sets of data.

A hyperbolic function which has been used to fit the stress–strain curves of soils [18, 19] and rocks [20] under triaxial compression has the following basic form:

$$\sigma = \frac{\epsilon}{A + B\epsilon} \tag{5}$$

where σ is the deviator stress, ϵ is the axial strain and A and B are constants. For the present type of curves, the following formula was adopted:

$$\sigma_n = \frac{\Delta V_j}{a - b\,\Delta V_j} \tag{6}$$

or, in linear form as

$$\frac{\Delta V_j}{\sigma_n} = a - b\,\Delta V_j. \tag{7}$$

Plots of $\Delta V_j/\sigma_n$ vs ΔV_j for a large number of data showed good linearity irrespective of the stress history, loading mode and type of joint. Figure 12 presents the plots of the data sets, which have been included in Fig. 11. Since both functions (4) and (6) describe a hyperbolic variation of ΔV_j with σ_n, it must be the formulation of (4) which exaggerates any small deviations of the experimental curves from an ideal hyperbola.

The normal stiffness (K_n) of a joint cannot be defined by a single value. For each increment of σ_n, the corresponding k_n value must be obtained from the derivative of (6), which may be rewritten as:

$$\sigma_n = \frac{1}{\dfrac{a}{\Delta V_j} - b} \tag{8}$$

which implies that for very large values of σ_n ($\rightarrow \infty$), ΔV_j must tend to the limiting value a/b, hence

$$\frac{a}{b} = \text{asymptote to the hyperbola} = V_m \text{ (max closure)}$$

Therefore, at V_m the tangent joint stiffness (K_n) will acquire an infinite value. For an extremely small increment of σ_n ($\rightarrow 0$), ΔV_j will also $\rightarrow 0$, and hence:

$$K_n = \frac{1}{a} = K_{ni}. \tag{9}$$

Therefore, the constant a represents the reciprocal of the initial normal stiffness (K_{ni}).

The values of K_{ni} and V_m uniquely define the hyperbolic stress–closure relation of a joint. The value of K_n at any level of σ_n may be found from the derivative of (6):

$$K_n = \frac{\partial \sigma_n}{\partial \Delta V_j} = \frac{1}{a\left(1 - \dfrac{b}{a}\Delta V_j\right)^2} = \frac{K_{ni}}{\left(1 - \dfrac{\Delta V_j}{V_m}\right)^2}. \tag{10}$$

By substitution of ΔV_j as:

$$\Delta V_j = \frac{\sigma_n a}{1 + \sigma_n a} = \frac{\sigma_n V_m}{K_{ni} V_m + \sigma_n} \tag{11}$$

equation (10) becomes:

$$K_n = K_{ni}\left[1 - \frac{\sigma_n}{V_m K_{ni} + \sigma_n}\right]^{-2}. \tag{12}$$

Both K_{ni} and V_m data of a particular joint are dependent upon the initial stress level (σ_i). In an experimental determination of those parameters, the joint can be precompressed under the estimated *in-situ* seating stress, before closure readings begin. Alternatively, when the experimental σ_i is zero, the compression curve may be obtained by translating the axes to a position (σ_i, ΔV_j), such that σ_i will correspond to the *in-situ* seating condition.

(b) *Unloading and irrecoverable closure*

Goodman [9] has suggested that the unloading curves for joints will follow essentially the same path as for the intact rock. The present work has shown that joint behaviour is not so simple as this (see the examples in Figs 3 and 4). A significant fact which emerged was that the unloading stress–opening curves for joints are also hyperbolic. Behaviour is governed by equation (6), as for

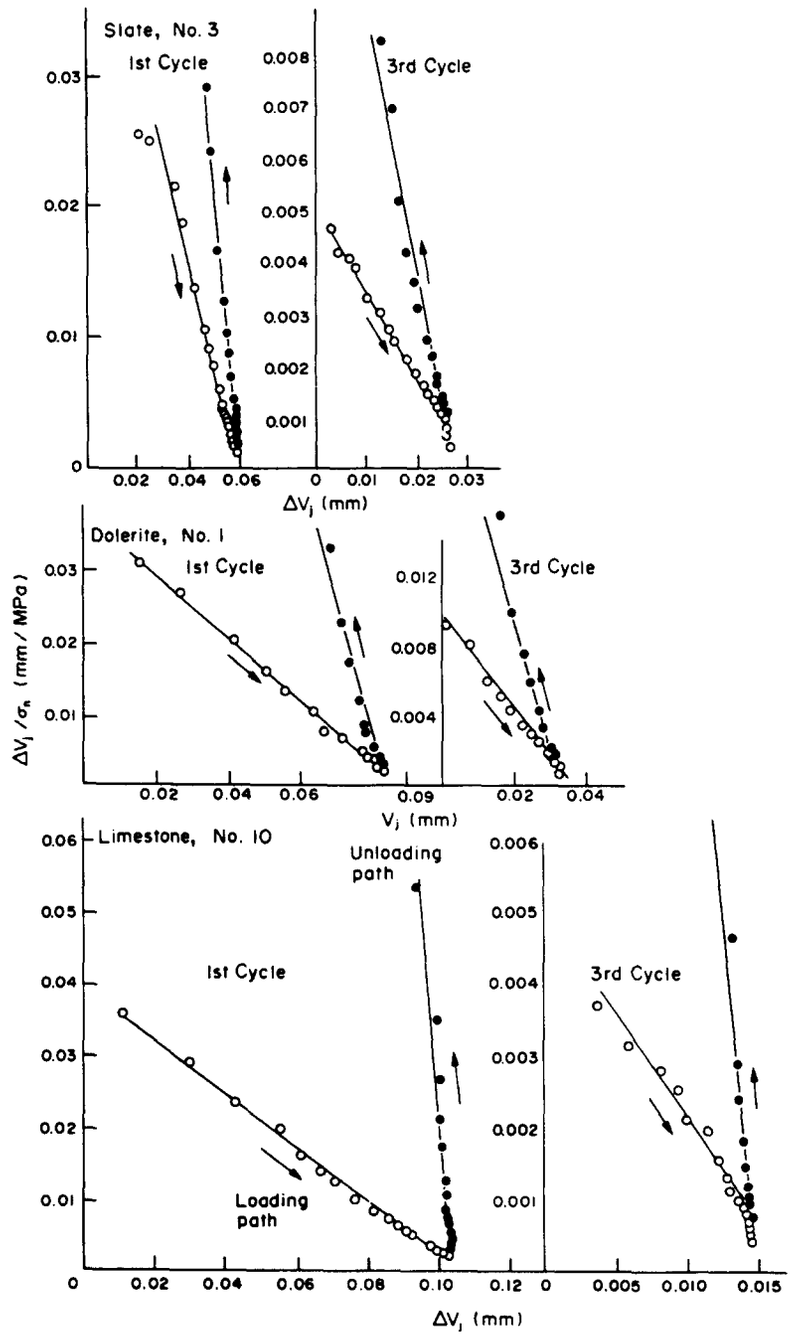

Fig. 12. Linear plots of $\Delta V_j/\sigma_n$ vs ΔV_j for different joint types, indicating good hyperbolic fit irrespective of the stress history and the loading mode.

loading, and linear relations are obtained when data is plotted in the form of equation (7)—see Fig 12 for typical examples.

An examination of the available data suggests that when the loading stages are taken to the maximum closure condition (i.e. to stress levels in the 40–50 MPa range), the hyperbolic unloading curves obtained from the first, second and third cycles are each of similar shape. However, this common shape is dissimilar to the unloading curve for the solid rock. This is to be expected in view of the different sample thicknesses and areas of contact involved. Joints exhibit much higher unloading stiffnesses than the solid rock, though if a sufficiently thin slice of solid rock were unloaded, the modes of behaviour would possibly converge somewhat.

(*ii*) *Dislocated joints*. Trials of various functions (hyperbolic, power, semi-log) showed that the semi-log fit could give the best approximation to the experimental compression curves of the dislocated joints. As shown in Fig. 13, plots of closure (ΔV_j) data vs logarithmically scaled σ_n gave good linear relations. A semi-log relation between σ_n and ΔV_j implies that a joint will never reach the maximum closure state, which is the case for dislocated joints.

The relations in Fig. 13 are expressed by:

$$\log \sigma_n = p + q \cdot \Delta V_j \tag{13}$$

which implies that for $\Delta V_j = 0$ (initial reference for taking closure measurements), $\log \sigma_n$ is equal to p. Hence, the intercept p represents the initial normal stress (σ_i). The antilog of the coefficients p in Fig. 13 indicate somewhat higher σ_i values (0.175–0.268 MPa) than the experimental ($\cong$0.15 MPa). This is the result of the slight deviation of the closure data from an ideal semi-log relation in the very low stress range.

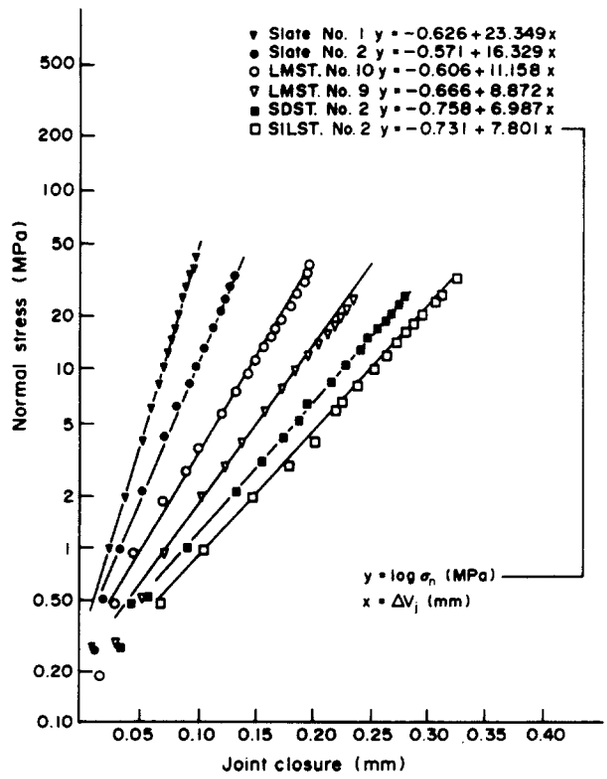

Fig. 13. Semi-log plots of normal stress vs closure of mismatched joints.

The incremental normal stiffness (K_n) for dislocated joints can be calculated from the derivative of function (13):

$$K_n = \frac{\partial \sigma_n}{\partial \Delta V_j} = \frac{q\sigma_n}{\log_{10} \cdot e} = \frac{q\sigma_n}{0.4343}. \tag{14}$$

(*c*) *Shear stress* (τ) *vs displacement* (d_h) *curves*

Hyperbolic functions are frequently used to express analytically the non-linear behaviour of sheared joints in the pre-peak range. Kulhaway [20] refers to the following formula:

$$\tau = \frac{d_h}{m + nd_h} \tag{15}$$

where d_h is the shear displacement at a level of shear stress τ, and m and n are the constants of the hyperbola. The constant (m) represents the reciprocal of the initial shear stiffness (K_{si}) and the constant (n) is the reciprocal of the horizontal asymptote (t_{ult}) to the hyperbolic $\tau - d_h$ curve. Development of (15) leads to:

$$K_{st} = K_j(\sigma_n)^{nj}\left(1 - \frac{\tau \cdot R_f}{\tau_p}\right)^2 \tag{16}$$

which describes the tangent shear stiffness (K_{st}) of a joint at any level of shear (τ) and normal (σ_n) stress. The various terms in equation (16) are:

K_j = stiffness number;
n_j = stiffness exponent;
R_f = failure ratio = τ/τ_{ult};
τ_p = peak shear strength.

Hungr and Coates [6] derived a relation uniquely defined by the "yield" point of the τ–d_h curves. The basic form of their function was:

$$\tau = \frac{ut}{t - d_h} - u, \text{ for } t < d_h \tag{17}$$

where u and t are constants, defined as follows:

$$u = -\frac{zaf\sigma_n^2}{a \cdot \sigma_n - b} \quad \text{and} \quad t = \frac{zfb}{a(a\sigma_n - b)} \tag{18}$$

where

z = ratio of the yield (τ_y) to the peak (τ_p) stress
a = ratio of the yield secant shear stiffness (K_{sy}) to normal stress (σ_n)
f = peak friction coefficient under σ_n
b = scale coefficient of plot axes x and y

According to equation (16), the incremental tangent shear stiffness (K_{st}) at any level of shear or normal stress can be calculated from:

$$K_{st} = \frac{ut}{(t - d_h)^2}. \tag{19}$$

Both functions (15) and (17) were tested against a large number of the present shear test data. It was found that both equations offer a good representation of the pre-peak shear behaviour irrespective of the joint type and level of normal stresses.

It is seen, therefore, that simple empirical functional relations may offer a realistic expression of the joint deformational behaviour under normal and shear loading conditions. The obvious advantage of such relations is that they are based on parameters which can easily be measured by experiment. For example, the changing stiffness of a joint under compression is uniquely defined by the initial stiffness and the maximum closure. Likewise, the changing stiffness of a joint in shear can be defined by the stiffness number (K_j), exponent (n_j) and failure ratio (R_f), etc. The functional relations can be incorporated in numerical analyses, e.g. in a finite element model modifying progressively the K_n and K_s values by incremental or iterative procedures to simulate non-linear stress–deformation behaviour.

PROCESSING OF THE EXPERIMENTAL DATA

As was shown earlier, the total deformation curve of a jointed block eventually becomes asymptotic to a line representing the elastic compression of the rock material.

Goodman and St. John [14] suggested that the maximum closure (V_m) can be approximated by the intersection of the asymptote to the joint block compression curve with the total deformation (ΔV_t) axis.

The function which was found to fit the experimental data best was a simply modified form of the hyperbolic expression (6) by addition of a linear component (ΔV_r):

$$\Delta V_t = \Delta V_j + \Delta V_r = \frac{\sigma_n a}{1+\sigma_n b} + \frac{\sigma_n}{C} \tag{20}$$

where C is a constant representing the elastic normal stiffness of the rock material. The experimental results were processed using a non-linear regression program in Algol 68 [21]. Each data set was fitted with:

$$\Delta V_t = \frac{1}{\dfrac{1}{\sigma_n a} + \dfrac{b}{a}} + \frac{\sigma_n}{C} \tag{21}$$

so that for very large σ_n, (21) becomes:

$$\Delta V_t = \frac{a}{b} + \left(\frac{1}{C}\right)\sigma_n \tag{22}$$

and thus, for large σ_n the slope was $1/C$ and the intercept was a/b, which has been defined as the maximum closure V_m. The uncertainty in the predicted V_m and K_{ni} values obtained by fitting equation (21) to the experimental loading paths was rarely outside the ± 1–4% range. In order to allow for the non-linear rock deformation component included in the predicted value of V_m, average correction quantities were determined experimentally for each rock type.

DISCUSSION OF THE RESULTS

Interlocked joint normal stiffness

A summary of the experimental results is presented in Table 3, and shows the ranges and average maximum closure (V_m) and initial normal stiffness (K_{ni}) values from all loading cycles.

Study of the V_m data in conjunction with the strength and geometrical properties of the joints showed that:

(a) the maximum closure (V_m) of joints with similar average aperture thickness (a_j) depended primarily on the strength of the joint walls (JCS). The large increase in the closure of the weathered joints was the result of the combined effect of wider a_j and much lower JCS. The combined effect of the latter two variables can be seen in Fig. 14, where V_m has been plotted against the ratio JCS/a_j for all the joints tested.

Curve fitting procedures applied to the relations in Fig. 14 showed that the data were fitted best by a power curve:

$$V_m = C\left(\frac{\text{JCS}}{a_j}\right)^D. \tag{23}$$

The values of the constants C and D and the coefficients of determination (r^2) were found to be:

1st loading:	$C_1 = 8.57$	$D_1 = -0.68$	$r_1^2 = 0.865$
2nd loading:	$C_2 = 4.46$	$D_2 = -0.65$	$r_2^2 = 0.599$
3rd loading:	$C_3 = 6.41$	$D_3 = -0.72$	$r_3^2 = 0.607$

The units of JCS and a_j are MPa and mm respectively;

(b) plots of V_m data vs Joint Roughness Coefficients (JRC) for joints with similar aperture thickness exhibited well defined trends of decreasing maximum closure with increasing JRC, irrespective of the Joint Wall Strength (JCS), as shown in Fig. 15. An explanation may be as follows: upon initiation of loading, joints undergo a rapid closure through readjustment of their initial seating condition. The more effective interlocking of rough surfaces reduces the amount of initial joint closure/readjustment. As σ_n increases, joint closure depends almost exclusively on the deformability of asperities. The tight mechanical interlock between the protrusions of a rough surface creates a very effective confined environment, thus stiffening the deformational response of the asperities.

The relations derived between the maximum closure (V_m) and the indices of wall aperture (a_j), strength (JCS) and roughness (JRC), were combined to yield an empirical function expressing the effect of all three variables on V_m:

$$V_m = A + B(\text{JRC}) + C\left(\frac{\text{JCS}}{a_j}\right)^D. \tag{24}$$

Multiple regression of all sets of data gave the following values for the constants:

$A_1 = -0.2960 \pm 0.1258$	$A_2 = -0.1005 \pm 0.0530$
$B_1 = -0.0056 \pm 0.0022$	$B_2 = -0.0073 \pm 0.0031$
$C_1 = -2.2410 \pm 0.3504$	$C_2 = -1.0082 \pm 0.2351$
$D_1 = -0.2450 \pm 0.1086$	$D_2 = -0.2301 \pm 0.1171$
$r_1^2 = 0.675$	$r_2^2 = 0.546$

Table 3. Summary of K_{ni} and V_m data from all interlocked joint types (initial stress $\sigma_{ni} = 1$ kPa)

Rock type and weathering state of joints	JCS (MPa)	No. of joints	Range and average V_m and K_{ni} data: 1st Cycle K_{ni} (MPa/mm) Range	1st Cycle K_{ni} Av.	1st Cycle V_m (mm) Range	1st Cycle V_m Av.	2nd Cycle K_{ni} (MPa/mm) Range	2nd Cycle K_{ni} Av.	2nd Cycle V_m (mm) Range	2nd Cycle V_m Av.	3rd Cycle K_{ni} (MPa/mm) Range	3rd Cycle K_{ni} Av.	3rd Cycle V_m (mm) Range	3rd Cycle V_m Av.
Slate														
Fresh	175	3	24.1–46.5	35.0	0.019–0.058	0.039	98.0–344.3	181.1	0.015–0.034	0.027	185.2–424.4	266.2	0.015–0.035	0.027
Moderately weathered	142	1	—	13.1	—	0.106	—	69.0	—	0.046	—	235.5	—	0.039
Weathered	77	3	11.6–13.8	12.7	0.290–0.384	0.331	19.1–40.0	32.6	0.095–0.207	0.146	49.5–77.6	63.6	0.069–0.165	0.118
Dolerite														
Fresh	167–182	2	21.7–26.7	24.2	0.084–0.117	0.101	59.0–75.3	67.1	0.045–0.061	0.053	102.9–119.4	111.2	0.042–0.092	0.067
Weathered	60–76	3	8.1–13.4	10.8	0.454–0.525	0.484	24.7–91.5	50.0	0.077–0.238	0.150	37.5–130.4	80.4	0.062–0.175	0.109
Limestone														
Fresh to slightly weathered	152–170	11	7.9–30.6	18.8	0.068–0.114	0.091	53.9–133.5	85.3	0.021–0.053	0.042	72.2–159.5	117.9	0.016–0.045	0.030
Moderately weathered	94–120	5	4.9–70.2	30.1	0.070–0.156	0.116	25.7–90.7	51.7	0.026–0.087	0.060	53.3–168.4	98.9	0.019–0.077	0.040
Weathered	35–53	5	3.8–12.9	8.5	0.307–0.525	0.373	39.8–49.4	44.2	0.070–0.124	0.115	42.5–65.2	56.9	0.059–0.114	0.079
Siltstone														
Fresh	105	5	14.0–25.9	18.9	0.117–0.152	0.135	21.8–64.2	43.9	0.039–0.099	0.072	21.8–69.7	53.5	0.040–0.096	0.063
Moderately weathered	67	2	10.5–11.2	10.8	0.281–0.339	0.310	20.0–21.6	20.8	0.132–0.277	0.205	19.9–25.9	22.9	0.130–0.237	0.184
Weathered	44	3	6.9–14.2	10.4	0.500–0.523	0.514	27.0–28.6	27.8	0.101–0.106	0.104	29.0–40.9	35.0	0.120–0.105	0.113
Sandstone														
Fresh to slightly weathered	68–95	8	3.6–22.7	12.8	0.128–0.246	0.170	11.5–34.9	23.4	0.043–0.156	0.075	18.3–62.1	37.2	0.024–0.096	0.054
Moderately weathered	64–58	9	4.3–25.6	9.3	0.197–0.286	0.240	8.8–26.9	17.9	0.064–0.156	0.101	14.8–44.8	26.7	0.057–0.139	0.089
Weathered	22	4	2.3–4.7	3.1	0.370–0.552	0.469	9.0–13.7	11.3	0.066–0.196	0.131	11.3–19.9	15.6	0.064–0.095	0.080

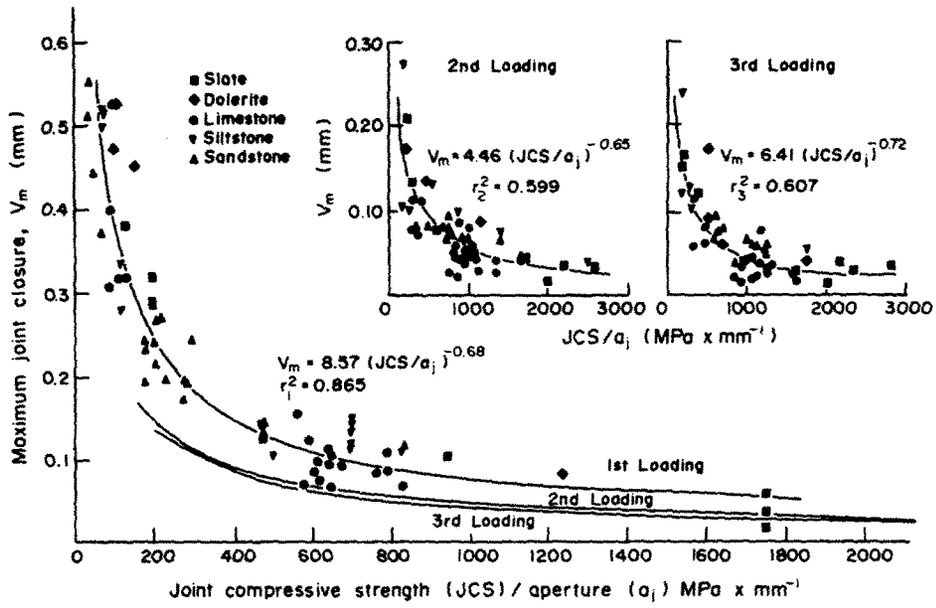

Fig. 14. Relations between maximum closure (V_m), wall strength (JCS) and aperture (a_j) of different joint types under repeated normal loading.

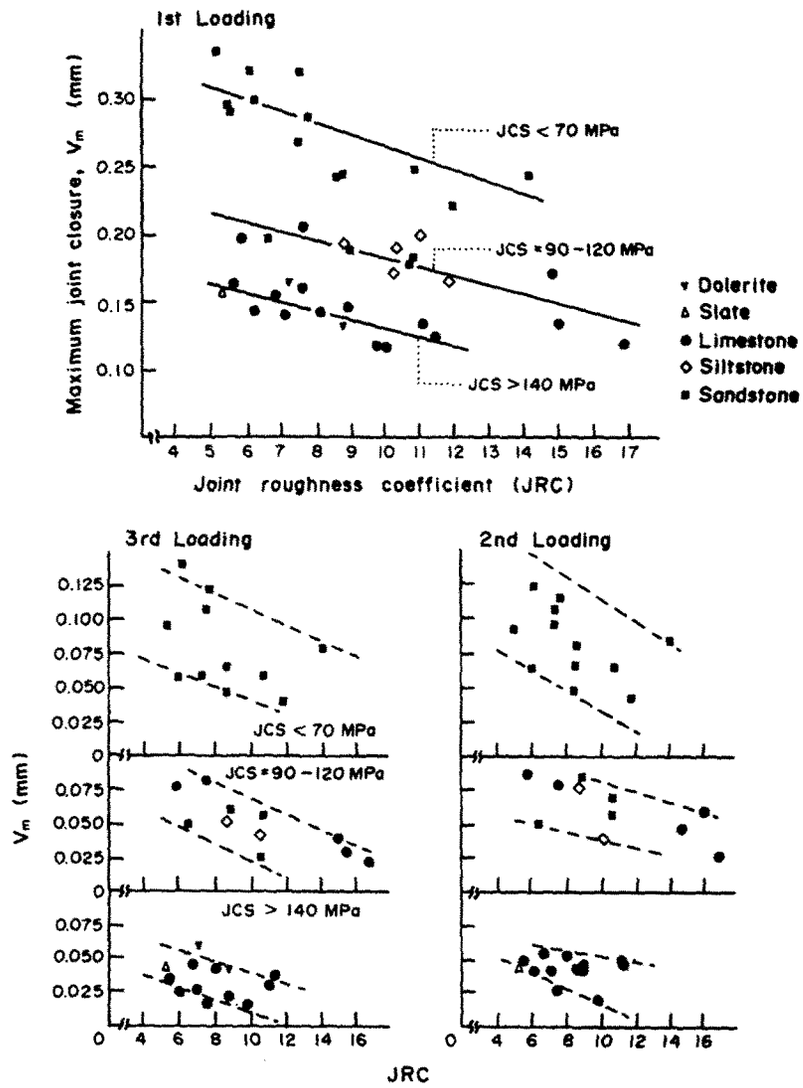

Fig. 15. Relations between maximum closure (V_m) and wall roughness (JRC) for different joint types.

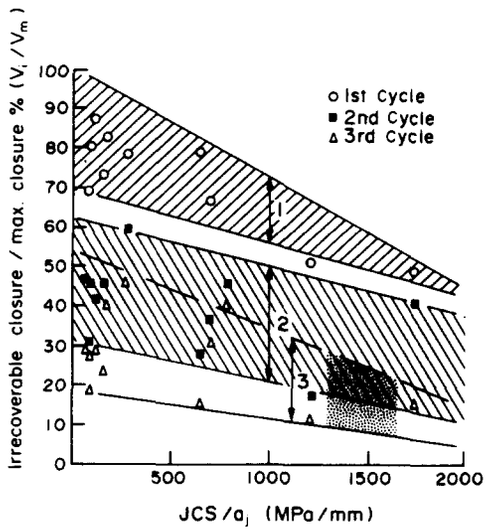

Fig. 16. Irrecoverable joint closure reduces with number of load cycles; with JCS_0 value; and with the smallness of the initial joint aperture (a_j).

$$A_3 = -0.1032 \pm 0.0680$$
$$B_3 = -0.0074 \pm 0.0039$$
$$C_3 = 1.1350 \pm 0.3261$$
$$D_3 = -0.2510 \pm 0.1029$$
$$r_3^2 = 0.589$$

Note:

(1) Subscripts 1, 2, 3 correspond to the cycle no.; $\pm$ = one standard deviation; r^2 = coefficient of determination

(2) The values of a_j for the second and third cycles are based on the initial aperture minus the permanent set at the end of the 1st and 2nd cycles, respectively.

The empirical function (24) represents a simple constitutive relation, describing the variations in V_m of unfilled interlocked joint types in the following range of wall strength and geometry indices:

$$JRC = 5\text{–}15$$
$$JCS = 22\text{–}182\ \text{MPa}$$
$$a_j = 0.10\text{–}0.60\ \text{mm}$$

and provided that σ_{ni} does not exceed 1 kPa.

The ability to predict V_m means that values of the asymptote (a/b) to the hyperbola (equation 6) can also be predicted. The value of the constant (a) is equal to the reciprocal of the initial normal stiffness (K_{ni}) and can be obtained from the following relation [13]:

$$K_{ni} = -7.15 + 1.75\,JRC + 0.02\left(\frac{JCS}{a_j}\right), \quad r^2 = 0.573. \quad (25)$$

Thus a complete stress–closure curve for a given joint can be predicted using equations (25) and (26) to obtain the appropriate constants for evaluating equation (6).

There are several as yet unresolved problems concerning loading and unloading behaviour of rock joints. It is difficult to predict the ratio of maximum closure (V_m) to initial aperture (a_j). The present data indicate values for the first load cycle in the range from 0.3–0.9, though generally average about 0.7. A fair approximation to the initial aperture (a_j) of a joint can be obtained from the following empirical relation:

$$a_j = \frac{JRC}{5}\left(0.2\frac{\sigma_c}{JCS} - 0.1\right) \quad (26)$$

derived from analysis of the present data, where

a_j = initial joint aperture in mm under self-weight stress ($\cong$ 1 kPa)

σ_c = uniaxial compressive strength

The ratio of irrecoverable closure (V_i) to maximum closure (V_m) for a given load cycle is also difficult to predict. The plot of the available data in Fig. 16 indicates considerable scatter, though consistent trends are apparent.

By applying equations (26) to predict a_j and (24) to predict V_m, our estimate of V_i can be obtained from the plots in Fig. 16.

As shown earlier, the unloading paths are adequately described by the hyperbolic function (6). The constants (a) and (b) required to define the unloading hyperbola for a given load cycle can be estimated from:

$$a/b \cong V_m - \Sigma V_i$$
$$a = 1/K_{ni}$$

Where K_{ni} is estimated from equation (25) with a_j replaced by ($a_j - \Sigma V_i$).

Table 4. Summary of interlocked and mismatched joint normal stiffness ratios (average and range)

Normal stress		K_n (interlocked)/k_n (mismatched) 0.5 (MPa)	5.0 (MPa)	15.0 (MPa)
High JRC	*High JCS* (4 spec.)	7.5 (4.5–10)	6.5 (4.5–10)	12.1 (7.7–20)
	Low JCS (6 spec.)	3.7 (1.4–5.6)	3.3 (2.1–7.7)	4.3 (3.0–6.6)
Low JRC	*High JCS* (5 spec.)	3.1 (2.0–7.7)	3.7 (2.9–11.8)	7.1 (5.3–12.5)
	Low JCS (8 spec.)	1.9 (1.1–2.9)	2.0 (1.4–2.4)	3.3 (2.8–4.0)

Note:
High JCS: 120–175 MPa (mean 156 MPa) *Low JCS*: 44–105 MPa (mean 70 MPa)
High JRC: 9.5–15 (mean 11.0) *Low JRC*; 4.0–7.6 (mean 6.4).

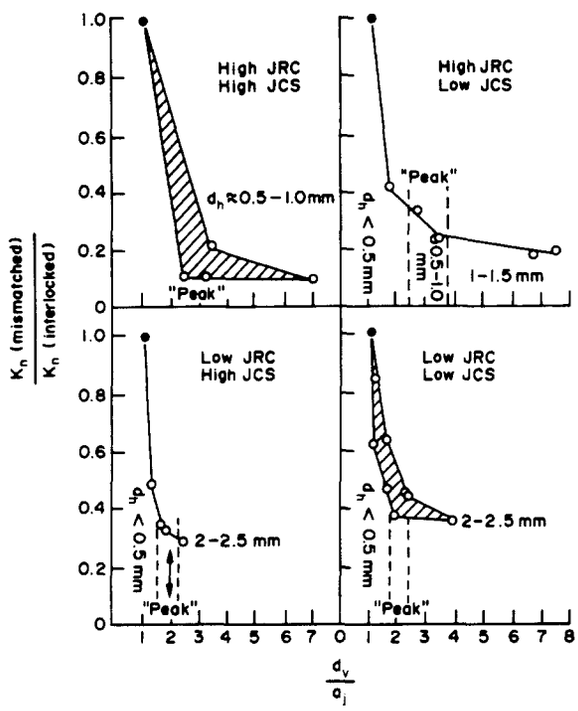

Fig. 17. Illustration of the changes in joint stiffness with joint "opening" at different stages of shear displacement, d_h.

Comparison between interlocked and dislocated joint normal stiffness

The purpose of mismatching the joint surfaces was to investigate, in a simplified manner, how normal stiffness was affected by shear displacement. This is an aspect of potential interest, because modelling of the complete joint behaviour requires data describing how K_n (interlocked) reduces as shearing takes place to d_h (peak) and thence to d_h (residual).

Comparison of the interlocked and dislocated normal stress–closure records of the same joint specimens indicated that the interlocked stiffness was several times higher. A summary of the results is shown in Table 4.

As expected, the highest stiffness ratios were obtained from joints of high JRC/high JCS and the lowest from the joints of low JRC/low JCS. The stiffness ratios generally show some increase with increasing level of normal stress due to the hyperbolic and semi-log variations in the closure of interlocked and mismatched joints respectively.

Increasing relative displacement results in progressively larger joint opening as the gradually reducing number of contact points are transferred higher onto the asperity slopes and the stiffness of the joint drops. An illustration of the changes in stiffness with shear displacement/joint opening is presented in Fig. 17 for the four groups of joints as given in Table 4. The relative amount of joint opening is defined by the ratio of the vertical uplift d_v of the upper block to the aperture of the joint when interlocked. The values of d_v and d_v/a_j depend on the surface roughness and the relative amount of shear.

Assuming peak displacements to be within 0.5–1.0 mm, the following three stages of joint shearing occur in Fig. 17: a pre-peak stage ($d_h \leqslant 0.5$ mm), the peak stage ($d_h \sim 0.5$–1.0 mm), and a post-peak stage ($d_h > 1.5$–2.5 mm). The plots indicate that an extremely small amount of dislocation from an originally interlocked position will cause a large reduction of the original stiffness, which could amount to up to 3/4 of the total reduction in stiffness from $d_h = 0$ to $d_h = d_{h(peak)}$. An assumption of linear decrease in $(K_n)_m/(K_n)_i$ with shear displacement from zero to $d_{h(peak)}$ would be sufficiently accurate for purposes of numerical simulation in the present state of knowledge. The following empirical relation indicates how the data presented in Table 4 can be used to modify the K_n (interlocked) data obtained from equation (12), to allow for the changes induced by shearing (mismatching):

$$\frac{K_{n(\text{int.})}}{K_{n(\text{mism.})}} \simeq 2 + \frac{\text{JRC}\cdot\text{JCS}\cdot\sigma_n}{2500}. \tag{27}$$

For example, if JRC = 10, JCS = 100 MPa, then for $\sigma_n = 1$ MPa and 10 MPa equation (27) predicts $K_{n(\text{int})}/K_{n(\text{mism})} \approx 2.4$ and 6 respectively.

Small post-peak displacements indicate a further reduction in stiffness, but at a much lower rate. It appears that an asymptote value is reached after a shear displacement several times the $d_{h(peak)}$ value.

Joint shear stiffness

The range of shear stiffness parameters derived from the experimental results are summarized in Table 5. Linear regression analysis of the d_h/τ vs d_h plots (see equation 15) yielded the initial shear stiffness coefficient (K_{si}) at each level of σ_n. The log-log relation between K_{si} and σ_n gave the values of the stiffness number (K_j) and stiffness exponent (n_j). As the failure ratio (R_f) values did not display larger differences under different σ_n, mean values are presented.

The variation in the secant peak shear stiffness (K_s) with normal stress is illustrated in Fig. 18. The stiffness envelopes invariably have curved shapes resembling the peak shear strength envelopes of joints. The non-linear variation of K_s with σ_n reflects the non-linear variation of τ_{peak} with σ_n and the small increases in $(d_h)_{peak}$ with increasing σ_n. Distinct changes in the gentle curvature of the stiffness envelopes are due to the multistage testing. The envelopes in Fig. 18 also demonstrate the dependency of peak shear stiffness on joint wall strength (JCS) and roughness (JRC). Based on similar observations, Barton and Choubey [22] suggested the empirical relation

$$K_s = \frac{100}{L}\sigma_n \tan\left[\text{JRC}\log_{10}\left(\frac{\text{JCS}}{\sigma_n}\right) + \phi_r\right] \tag{28}$$

to describe the variation of K_s with the aforementioned joint variables where L is the joint length introduced to allow for the scale effect on K_s. The equation is based on the assumption that peak shear strength is reached after shearing approximately 1% of the joint length. In view of the potential existence of a critical joint length L_c controlled by the average cross-joint spacing [23] the

Table 5. Summary of the experimental joint shear stiffness parameters

Rock type	Weathering state of joint samples	Range of normal stress (MPa)	Initial K_{si} (MPa)	Stiffness k_j (MPa/mm)	Stiffness exponent (n_j) (MPa)^2/mm	Failure ratio R_f	Secant peak K_s (MPa/mm)
Sandstone	Fresh (3 samples)	0.25–2.36	2.2–37.6	13.02	0.674	0.748	0.56–4.50
	Slightly weathered (1 sample)	0.25–2.07	8.7–41.9	24.49	0.714	0.738	1.23–4.74
	Moderately weathered (2 samples)	0.24–2.04	1.2–6.2	3.88	0.725	0.810	0.47–1.73
	Weathered (3 samples)	0.50–1.96	2.1–6.5	3.49	0.831	0.887	0.56–1.35
Limestone	Slightly weathered (1 sample)	0.23–1.84	8.0–50.5	30.19	0.799	0.830	1.65–6.87
	Moderately weathered (1 sample)	0.24–1.90	4.1–17.3	9.73	0.698	0.731	1.12–3.13
	Weathered (1 sample)	0.25–1.53	1.0–10.5	5.04	1.118	0.788	0.66–1.89
Dolerite	Slightly weathered (1 sample)	0.26–2.11	8.2–19.0	17.74	0.615	0.652	1.75–4.98
	Weathered (1 sample)	0.28–1.11	3.6–9.1	9.02	0.674	0.778	0.86–2.19
Slate	Fresh (3 samples)	0.54–2.28	$=K_s$	—	0	0	5.6–12.6
	Weathered (3 samples)	0.40–1.45	2.8–7.5	5.72	0.760	0.870	0.64–1.27

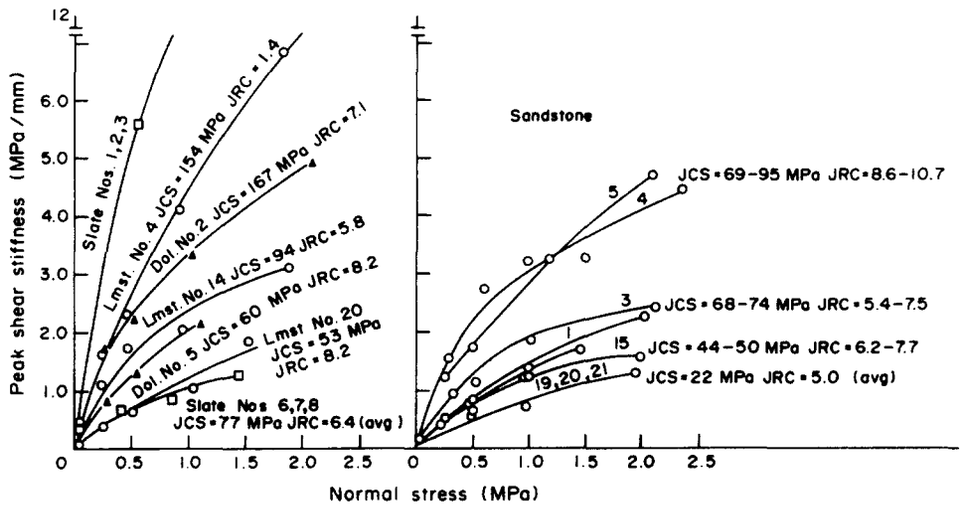

Fig. 18. Variation in the peak shear stiffness (secant values) of different joint types with normal stress.

value of L in equation (28) should be adjusted accordingly.

The indices R_f, n_j and K_j which describe the non-linearity in joint behaviour showed the following characteristics:

(i) the failure ratio (R_f) ranging from 0.652–0.887 indicated that lower R_f values were associated with well interlocked, unweathered joints of high JRC*. Planar fresh, and especially weathered, joints gave the relatively higher values;

(ii) the stiffness exponent n_j (slope of the log-log relation between initial shear stiffness K_{si} and σ_n) was very similar, irrespective of joint type;

(iii) the stiffness number K_j (intercept of the above relation) varied significantly from 3.49 to 30.19 MPa/mm. This can, of course, be anticipated considering the variations in K_{si} and the essential similarity in the n_j values. Correlation of the K_j values with JRC showed a proportional linear trend. This is logical since the initial stiffness of a mated joint depends on the degree of interlocking, which in turn, is related with JRC. The best fit line for the thirteen available K_j values was

$$K_j = -17.19 + 3.86\,\mathrm{JRC} \qquad (29)$$

$$(r = 0.835, \text{ for } \mathrm{JRC} > 4.5).$$

* For linear stress–displacement relations, R_f is zero.

Anisotropy in joint deformability

A related feature of jointed rock masses that distinguishes continuum and discontinuum behaviour is the anisotropic deformability. Joint stiffness is much lower in the tangential than in the normal direction. The value of normal-to-peak shear stiffness ratio is not a constant but depends on the level of normal stress, the highest anisotropy being shown at low stresses, as shown in Fig. 19. It is seen that under extremely low σ_n (0.02–0.05 MPa) the K_n/K_s ratio attained maximum values ranging from 58 to 130. Within the σ_n range from 0.25 to 1 or 2 MPa, anisotropy was markedly reduced.

No universal conclusions could be drawn regarding the effect of weathering on joint anisotropy. In the case of the weathered joints in sandstone and dolerite, the K_n/K_s values were lower than for the fresh surfaces. For the cleavage planes in slate, anisotropy appeared similar in both fresh and weathered specimens, whereas the weathered limestone joint gave higher K_n/K_s values than the fresh surfaces.

CONCLUSIONS

This experimental study has enabled several conclusions to be drawn regarding the qualitative and quantitative characteristics of rock joint deformation.

From the qualitative standpoint, the following have been observed:

(1) The closure (ΔV_j) of joints varies non-linearly with normal stress (σ_n) throughout repeated loadings and irrespective of the rock and joint type. Under increasing σ_n, the joints gradually reach a state of maximum closure (V_m), whose value is directly dependent upon the previous stress history.

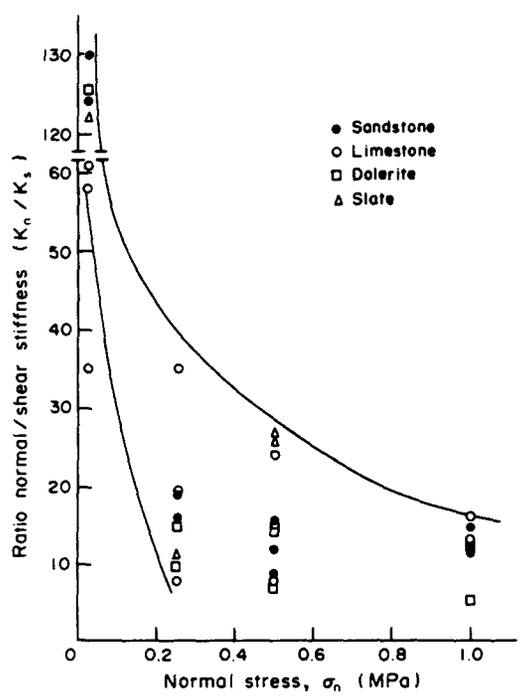

Fig. 19. Anisotropic joint behaviour under normal and shear loading.

(2) Upon unloading, the joints exhibit marked hysteresis and large permanent sets. A certain amount of recovery also occurs because of the elastically deformed asperities. After subsequent reloadings, the permanent set is considerably lower. However, it seems that several more cycles than the three applied in the present tests would be needed to obtain a single reproducible stress–closure curve.

(3) Dislocated (mismatched) point-contacting joints under normal loading present non-linear stress–deformation behaviour. The difference between interlocked and mismatched joint normal stiffness can be significant depending on the amount of joint opening and on the joint wall strength.

(4) The shear stress–shear deformation relations of joints in the pre-peak range reveal variable non-linear behaviour. Non-linearity is more profound in cases of weathered joint surfaces and least in cases of tightly interlocked fresh joints. The present tests indicate that the shear stress–deformation behaviour may be closer to the conceptual 'constant displacement' model, at least within the range of normal stresses of engineering interest.

From the analytical standpoint, the findings can be summarized as:

(5) Use of hyperbolic functions enables an accurate analytical representation of the normal stress (σ_n) vs closure (ΔV_j) curves of natural interlocked joints. Equation (6) was found to give the best fit to the present experimental curves, irrespective of the joint type, stress history and loading mode.

(6) The normal stress (σ_n) vs closure (ΔV_j) relation of dislocated joints is best described by a semilogarithmic function (equation 13).

(7) Non-linear shear stress (τ) vs displacement (d_h) curves in the pre-peak range can be adequately represented by hyperbolic functions (equations 15 or 17).

Finally, the practical/quantitative findings are summarized as:

(8) The analysis of the data has led to an inverse exponential relation between the maximum joint closure (V_m) and the ratio of wall strength (JCS) to average aperture thickness (a_j). Equation (23) gave the best fit.

(9) An inverse linear relation exists between maximum closure (V_m) and wall roughness (JRC), which combined with equation (23) gave a simple constitutive relation (equation 24), describing V_m as a function of a_j, JRC, JCS. Combination of a derived series of related functions (24, 25, 26) enables prediction of the complete normal stress–deformation (closure/opening) behaviour of a joint.

(10) The normal stiffness of joints reduces significantly during the process of shearing. The largest part of the reduction in K_n occurs during the very initial stages of displacement. Subsequent changes up to d_{hp} and immediately after appear to occur at a considerably slower rate. Based on the present data, the empirical function (27)

gives an approximation of the reduction in K_n at the peak shear strength.

(11) The normal (K_n) to shear (K_s) stiffness ratio varies with normal stress, the highest anisotropy generally occurring under very low stress levels. No systematic effects of weathering on the K_n/K_s ratios have been identified.

Received 27 *August* 1982; *revised* 15 *July* 1983.

REFERENCES

1. Goodman R. E., Taylor R. L. and Brekke T. A model for the mechanics of jointed rock. *J. Soil Mech. Fdns Div., Proc. Am. Soc. civ. Engrs* **94(SM3)**, 637–659 (1968).
2. Goodman R. E. The mechanical properties of joints. *Proc. 3rd Congr. ISRM*, Denver, Vol. 1A, pp. 127–140 (1974).
3. Shehata W. M., Ph.D. thesis (1971), quoted in Sharp J. C. and Maini Y. N. T., in fundamental considerations on the hydraulic characteristics of joints in rock. *Proc. Symp. on Percolation Through Fissured Rock*, paper No. Tl-F, Stuttgart (1972).
4. Pratt H. R., Black A. D. and Brace W. F. Friction and deformation of jointed quartz diorite. *Proc. 3rd Congr. ISRM*, Denver, Vol. IIA, pp. 306–310 (1974).
5. Iwai K. Fundamental studies of fluid flow through a single fracture, Ph.D. thesis, Univ. of California, Berkeley, 208 pp (1976).
6. Hungr O. and Coates D. F. Deformability of rock joints and its relation to rock foundation settlements. *Can. Geotech. J.* **15**, 239–249 (1978).
7. Snow D. T. Fundamentals and *in-situ* determination of permeability. *Proc. Symp. on Percolation Through Fissured Rock*, paper Gl, Stuttgart (1972).
8. Infanti N. and Kanji M. A. *In situ* shear strength, normal and shear stiffness dfeterminations at Agua Vermelha Project. *Proc. 3rd Int. Congr. of IAEG*, Madrid, Vol. 2, pp. 175–183 (1978).
9. Goodman R. E. *Methods of Geological Engineering in Discontinuous Rock*, p. 472. West, New York (1976).
10. Kulhaway F. H. Geomechanical model for rock foundation settlement. *J. Geotech. Div., Proc. Am. Soc. civ. Engrs* **106(GT2)**, 211–227 (1978).
11. John K. W. Civil engineering approach to evaluate strength and deformability of regularly jointed rock. *Proc. 11th Symp. on Rock Mechanics*, pp. 68–82 (1970).
12. Rosso R. S. A comparison of joint stiffness measurements in direct shear, triaxial compression and *in situ*. *Int. J. Rock Mech. Min. Sci. & Geomech. Abstr.* **13**, 167–172 (1976).
13. Bandis S. C. Experimental studies of scale effects on shear strength and deformation of rock joints, Ph.D. thesis, Univ. of Leeds, 385 pp (1980).
14. Goodman R. E. and St. John C. Finite element analysis for discontinuous rock. In *Numerical Methods in Geotechnical Engineering*, Chap. 4, pp. 148–175. West, New York (1977).
15. Bandis S. C., Lumsden A. C. and Barton N. R. Experimental studies of scale effects on the shear behaviour of rock joints. *Int. J. Rock Mech. Min. Sci. & Geomech. Abstr.* **18**, 1–21 (1981).
16. Barton N. R. Review of a new shear strength criterion for rock joints. *Engng Geol.* **7**, 579–602 (1973).
17. Barton N. R. Modelling rock joint behaviour from *in situ* block tests—Implications for nuclear waste repository design. Technical Report 81-83, Terra Tek, Salt Lake City (1981).
18. Kondner R. L. Hyperbolic stress–strain response:cohesive soils. *J. Soil Mech. Fdns Div., Proc. Am. Soc. civ. Engrs* **89(SM1)**, 115–143 (1963).
19. Duncan J. M. and Chang C. Y. Non-linear analysis of stress and strain in soils. *J. Soil Mech. Fdns Div., Proc. Am. Soc. civ. Engrs* **96(SM5)**, 1629–1653 (1970).
20. Kulhaway F. H. Stress-deformation properties of rock and rock discontinuities. *Engng Geol.* **8**, 327–350 (1975).
21. Powel R. Personal communication (1978).
22. Barton N. R. and Choubey V. The shear strength of rock joints in theory and practice. *Rock Mech.* **10**, 1–54, (1977).
23. Barton N. R. and Bandis S. C. Some effects of scale on the shear strength of joints. *Int. J. Rock Mech. Min. Sci. & Geomech. Abstr.* **17**, 69–73 (1980).